International Journal of Nanomedicine

Dovepress
open access to scientific and medical research

Open Access Full Text Article

ORIGINAL RESEARCH

Multi-Site Attack, Neutrophil Membrane-Camouflaged Nanomedicine with High Drug Loading for Enhanced Cancer Therapy and Metastasis Inhibition

Ran Huang[1,*], Daopeng Fan[1,*], Hanghang Cheng[1], Jian Huo[1], Shuqi Wang[1], Hua He[1], Gaiping Zhang[1,2]

[1]College of Veterinary Medicine, International Joint Research Center of National Animal Immunology, Henan Agricultural University, Zhengzhou, 450046, People's Republic of China; [2]Longhu Laboratory, Zhengzhou, 450046, People's Republic of China

*These authors contributed equally to this work

Correspondence: Hua He, College of Veterinary Medicine, International Joint Research Center of National Animal Immunology, Henan Agricultural University, Zhengzhou, 450046, People's Republic of China, Email hehua1123@126.com; Gaiping Zhang, College of Veterinary Medicine, International Joint Research Center of National Animal Immunology, Henan Agricultural University, Zhengzhou, 450046, People's Republic of China, Email zhanggaip@126.com

Background: Advanced breast cancer is a highly metastatic tumor with high mortality. Simultaneous elimination of primary tumor and inhibition of neutrophil-circulation tumor cells (CTCs) cluster formation are urgent issues for cancer therapy. Unfortunately, the drug delivery efficiency to tumors and anti-metastasis efficacy of nanomedicine are far from satisfactory.

Methods: To address these problems, we designed a multi-site attack, neutrophil membrane-camouflaged nanoplatform encapsulating hypoxia-responsive dimeric prodrug hQ-$MMAE_2$ (hQNM-PLGA) for enhanced cancer and anti-metastasis therapy.

Results: Encouraged by the natural tendency of neutrophils to inflammatory tumor sites, hQNM-PLGA nanoparticles (NPs) could target delivery of drug to tumor, and the acute hypoxic environment of advanced 4T1 breast tumor promoted hQ-$MMAE_2$ degradation to release MMAE, thus eliminating the primary tumor cells to achieve remarkable anticancer efficacy. Alternatively, NM-PLGA NPs inherited the similar adhesion proteins of neutrophils so that NPs could compete with neutrophils to interrupt the formation of neutrophil-CTC clusters, leading to a reduction in extravasation of CTCs and inhibition of tumor metastasis. The in vivo results further revealed that hQNM-PLGA NPs possessed a perfect safety and ability to inhibit tumor growth and spontaneous lung metastasis.

Conclusion: This study demonstrates the multi-site attack strategy provides a prospective avenue with the potential to improve anticancer and anti-metastasis therapeutic efficacy.

Keywords: neutrophil membrane, high drug loading, hypoxia-responsive, CTC-neutrophil cluster, cancer and anti-metastasis therapy

Introduction

Metastasis is one of the major causes of cancer death in the clinic. Metastasis is a sequential process where tumor cells disseminate from primary tumor, known as circulating tumor cells (CTCs), and further extravasate to multiple organs to develop metastatic nodes.[1] Especially, advanced breast cancer (ABC) is one of highly metastatic tumor types, and 90% of mortalities are caused by metastasis, such as lung or bone metastasis.[2] Common cancer treatment modalities, such as chemotherapy and surgical resection, have demonstrated great potential in eradicating primary tumors, yet metastasis and post-operative recurrence remain a challenge that should be addressed. Recently, nanomedicine has drawn great attention in terms of cancer therapy because of their exceptional abilities, such as solubility, controlled drug release and safety.[3–5] However, the drug delivery efficiency to tumors (ie, drug loading and tumor targeting) and anti-metastasis efficacy of nanomedicine are far from satisfactory.[6,7] Therefore, an effective approach should be

Received: 31 March 2023
Accepted: 14 June 2023
Published: 20 June 2023

established for simultaneous elimination of primary tumor and inhibition of CTC dissemination to achieve enhanced cancer therapy.

As we have known, neutrophil plays an important role in tumor progression and metastasis. The tumor microenvironment has unique physiological characteristics compared to normal tissues, such as chronic inflammatory environment.[8] Based on their natural capability, neutrophils can be recruited to the inflammatory microenvironment of tumor, thus forming neutrophil extracellular traps (NETs) to promote the tumor growth.[9,10] On the other hand, neutrophils can also interact with CTCs to form neutrophil-CTC clusters, which are mediated by binding of vascular cell adhesion molecule 1 (VCAM1) on CTCs to integrins on neutrophils.[11,12] Based on the CTC-neutrophil-endothelial interaction, neutrophils contribute to CTC adhesion to endothelial cells, thus assisting CTC extravasation to form metastases.[13,14] All these evidences reveal that neutrophils possess natural targeting ability towards tumor sites, and neutrophil-CTC clusters are the key therapeutic objective for anti-metastasis therapy.[15]

In recent years, cell membrane-coated nanoparticles (NPs) have gained great attention as a promising therapeutic platform for cancer therapy.[16–19] Through using natural cell membranes to camouflage synthetic cores,[20] the NPs can successfully inherit the biological properties of the source cells, such as long circulation, active tumor targeting and binding ability,[21] thus achieving perfect anticancer efficacy.[22–24] Although nanomedicine can enhance tumor accumulation of chemo-drug via enhanced permeability and retention (EPR) effect and targeting moiety decoration,[25,26] limited nanomedicine has been used in clinical research, mainly because of tumor heterogeneity and complicated preparation method.[27–29] By comparison, based on the natural tendency of neutrophils to inflammatory tumor sites, neutrophil membrane coated NPs can act as a promising delivery system to improve targeted chemodrug delivery to tumor sites.[9] For another, neutrophil membrane coated NPs can also serve as a strong competitor for neutrophils to interact with CTCs, thus resulting in reduced formation of neutrophil-CTC clusters and inhibition of tumor metastasis.

How to achieve high drug loading and specific drug release are the major challenges for nanomedicine to eradicate the primary tumors. Due to π–π interactions between drugs, small molecule drugs would aggregate and precipitate during encapsulation, thereby leading to most nanomedicine with low drug loading (<10%) and premature drug leakage during the systemic circulation.[30] To address these problems, prodrugs,[31,32] especially dimeric prodrugs, have been extensively investigated,[33,34] in which the linkers in dimeric prodrug can weaken the strong intermolecular drug interactions, thus resulting in improving the drug loading capacity of nanomedicine.[35] On the other hand, to realize maximized anticancer efficacy and safety, various stimuli-responsive prodrugs have been designed to control specific drug release in tumor sites.[36–38] For example, hypoxia is a common pathological phenomenon at the late stage of tumor growth,[39,40] which is mainly caused by the abnormal vascular networks that are unable to supply sufficient oxygen. Based on the serious hypoxic level in the late-stage tumors, hypoxia-responsive dimeric prodrugs can be developed to realize high drug loading and hypoxia triggered drug release,[41] thereby resulting in effective anticancer treatment.[42]

Herein, we designed a multi-site attack nanomedicine against primary tumor and neutrophil-CTC clusters for enhanced cancer and anti-metastasis therapy (Scheme 1). First, the hypoxia responsive, quinone-modified monomethyl auristatin E (MMAE) dimeric prodrug (hQ-$MMAE_2$) was encapsulated into poly(D, L-lactide-co-glycolide) (PLGA) NPs to realize high drug loading of NPs.[43–46] Furthermore, neutrophil membrane was then coated onto the surface of PLGA NPs (hQNM-PLGA), which rendered PLGA NPs with biological properties of neutrophils, such as tumor accumulation, adhesion ability to CTCs. After i.v. injection, hQNM-PLGA NPs could be recruited to the inflammatory tumor site based on the inherent functions of neutrophils, thus leading to improved NPs stability, tumor accumulation, and minimal MMAE leakage during the systemic circulation. Under the serious hypoxic environment of advanced breast cancer, the hQ-$MMAE_2$ would degrade to facilitate MMAE release, thus resulting in achieving notable anticancer treatment. Alternatively, hQNM-PLGA NPs could effectively compete with neutrophils to interact with CTCs, thereby preventing the formation of neutrophil-CTC clusters and further inhibiting tumor metastasis. This multi-site attack, biomimetic nanomedicine with high drug loading provides a promising approach for metastasis inhibition and cancer treatment.

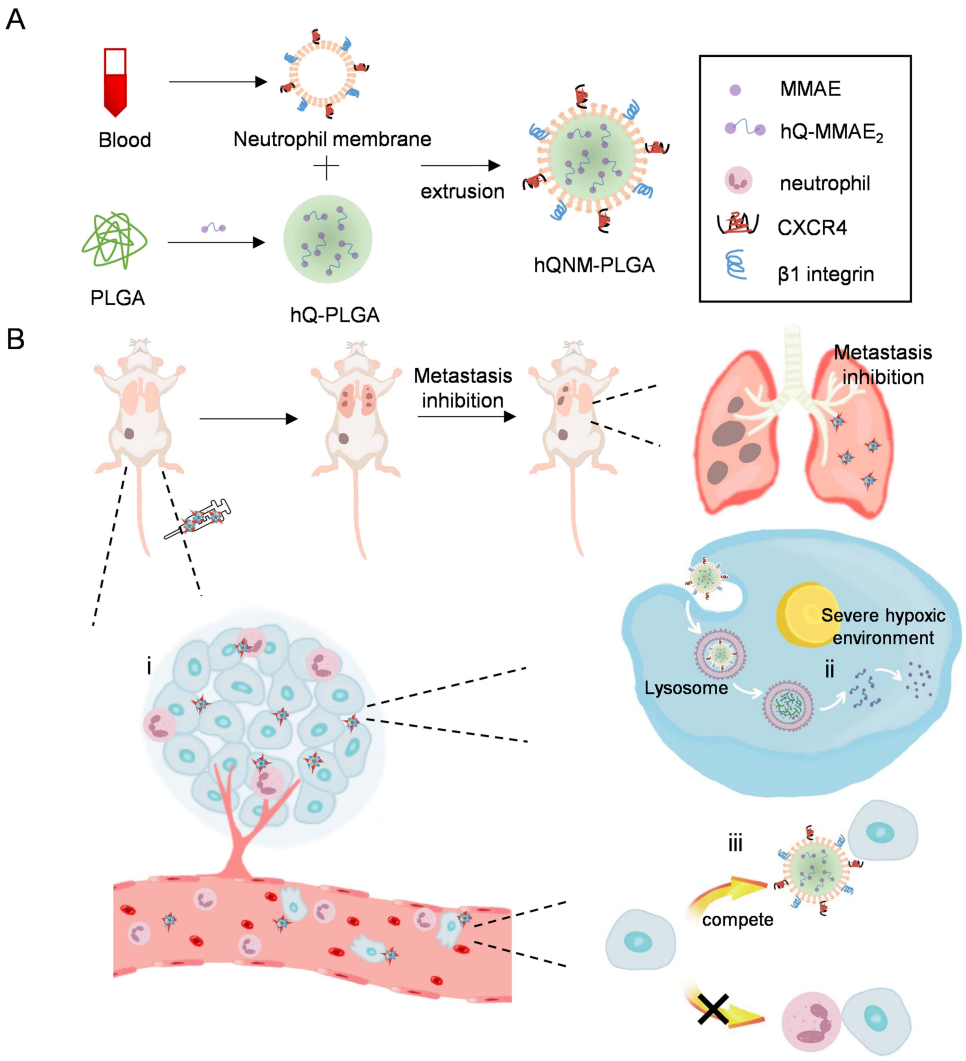

Scheme 1 Schematic illustration of multi-site attack, neutrophil membrane-camouflaged PLGA NPs encapsulating hypoxia-responsive dimeric prodrug for enhanced cancer and anti-metastasis therapy. (**A**) The hQNM-PLGA NPs were prepared via emulsion method, which contained neutrophil membranes and hypoxia-responsive dimeric prodrug hQ-$MMAE_2$. (**B**) (i) hQNM-PLGA NPs could target hQ-$MMAE_2$ delivery to tumor sites. (ii) hQ-$MMAE_2$ degraded in the hypoxic environment to facilitate MMAE release, thereby eliminating the primary tumor cells to achieve good safety and anticancer therapy. (iii) hQNM-PLGA NPs disrupted the neutrophils-tumor cells clusters formation, thus inhibiting tumor lung metastasis.

Materials and Methods

Materials, Cells and Animals

Chemicals were purchased from J&K (Beijing, China). Poly(D, L-lactide-co-glycolide) (PLGA, 50:50, Mw = 5000–15,000 Da) was purchased from Dalian Meilun Biotechnology Co. LTD (Dalian, China). Histopaque-1077 was purchased from Sigma-Aldrich (St Louis, MO, USA). Coumarin-6 and sodium cholate were purchased from Aladdin (Shanghai, China). MTT, one step TUNEL apoptosis assay kit and BCA kit were purchased from Beyotime® Biotechnology (Shanghai, China). Anti-CXCR4 and anti-Integrin beta 1 were all purchased from Abcam (Cambridge Science Park, UK). Anti ATP1A1 was purchased from BOSTER (Wuhan, China). PE Anti-Mouse Ly-6G/Ly-6C (Gr-1) was purchased from Proteintech (Wuhan, China). MMAE was purchased from Macklin (Shanghai, China). All solvents were purchased from Sinopharm Chemical Reagent Co. Ltd (Shanghai, China).

4T1 (mouse mammary carcinoma) and human umbilical vein endothelial cell (HUVEC) were obtained from ATCC (Rockville, MD) and cultured in RPMI-1640 medium containing 10% fetal bovine serum (FBS). Female BALB/c mice (6–8 weeks) were purchased from Animal experimental center of Huaxing (Zhengzhou, China) and housed in clean room. All animal studies were approved by the Institutional Animal Care and Use Committee, Henan Agricultural

University, and were performed in accordance with the Guidelines on Laboratory Animal Welfare issued by Ministry of Science and Technology of the People's Republic of China.

hQ-MMAE$_2$ Degradation

The synthetic route and characterization of hQ-MMAE$_2$ are described in Scheme S1. hQ-MMAE$_2$ was incubated in the mixture solution (acetonitrile/PBS, v/v=1/1, 200 μL) containing 10 mM $Na_2S_2O_4$. After centrifugation (10,000 rpm, 5 min) at the designated time, the supernatant was diluted with acetonitrile (400 μL) followed by HPLC analysis.

Preparation of Neutrophil Membrane

The neutrophil membrane (NM) was extracted according to a previous report.[47,48] Blood (1 mL) was collected from BALB/c mice, and further diluted with hank's balanced salt solution (HBSS, v:v, 1:10). After adding histopaque-1077 (11 mL), the mixture was centrifuged (4 °C, 400 g) for 45 min, the middle cloudy layer being neutrophils. After removal of the cloud layer, erythrocytes were lysed on ice for 10 min, centrifuged and resuspended using isolation buffer-1 to obtain neutrophils.

The neutrophils were suspended in isolation buffer-1, and sonicated for 2 min on ice. After centrifugation at 1000 g for 5 min, 10,000 g for 20 min, 100,000 g for 1 h, the precipitate was resuspended in ultrapure water and lyophilized to obtain neutrophil membrane (NM). The collected layer enriched with neutrophils was submitted to flow cytometry. The purity of the obtained neutrophils determined by flow cytometric analysis was 60.3% (Figure S1).

Preparation and Characterization of Nanoparticles (NPs)

PLGA and hQ-MMAE$_2$ were dissolved in dichloromethane (DCM) at a concentration of 10 mg/mL and 5 mg/mL, respectively. A mixture of PLGA (1 mL) and hQ-MMAE$_2$ (886 μL) was mixed with 1% sodium cholate solution (2 mL), sonicated at 20,000 J for 80s, and further added into 0.5% sodium cholate solution (10 mL) to evaporate DCM under stirring.[49,50] After centrifugation (14,500 rpm, 4 °C) for 50 min, the precipitate was collected and resuspended in ultrapure water to obtain PLGA/hQ-MMAE$_2$ (hQ-PLGA) NPs. To obtain the neutrophil membrane coated NPs, the neutrophil membrane (NM, 10 mg) was mixed with hQ-PLGA NPs, and the mixture was further extruded 20 times by the Avanti Polar Lipids to obtain neutrophil membrane coated, hQ-MMAE$_2$-loaded PLGA (hQNM-PLGA) NPs.[51] The neutrophil membrane coated, Cou6-loaded PLGA (CNM-PLGA) NPs, and neutrophil membrane coated, DiR-loaded PLGA (DNM-PLGA) NPs were prepared using the same method.

To verify the membrane-associated proteins on the NPs, neutrophils, NM and NM-PLGA NPs were lysed in RIPA lysis buffer for 20 min on ice. After centrifugation (4 °C, 13,000 g) for 10 min, the supernatant was used to analyze protein expression by SDS-PAGE and Western blot (anti-CXCR4 antibody, 1:500; anti-β1 integrin antibody, 1:2000).[52] The instrumentation used for the exposure and visualization of the Western blots was Amersham Imager 680.

The size and zeta potential were determined by dynamic light scattering (DLS), and the morphology was examined under transmission electron microscope (TEM). To evaluate the stability of NPs, hQNM-PLGA NPs and hQ-PLGA NPs were incubated at room temperature (RT) for various time before the measurement of the particle size. To investigate the drug loading content (DLC) and drug loading efficiency (DLE) of NPs, hQNM-PLGA NPs (100 μL) were added to acetonitrile (2.9 mL) and shaken at 220 rpm overnight. The DLC and DLE of hQ-MMAE$_2$ were determined by HPLC using acetonitrile/water mixture as the mobile phase (0.1 mL/min, λ_{abs} = 254 nm, Figure S2).

Hypoxia-Induced MMAE Release in vitro and in vivo

To evaluate the intracellular MMAE release under hypoxic condition, 4T1 cells were seeded at 1×10^5 cells/well on 12-well plates and incubated overnight. hQNM-PLGA NPs (200 nM MMAE) were added and incubated for 4 h, 8 h, or 12 h under different oxygen levels (20%, 10%, 5%). Cells were collected, lysed with RIPA lysis buffer at RT for 20 min, and sonicated on ice. The MMAE was extracted with a mixture solution (methanol/DCM = 1/1, v/v) at −20 °C overnight. After centrifugation (10,000 rpm, 4 °C) for 30 min, the MMAE in the supernatant was subjected to HPLC analysis (λ_{abs} = 210 nm).

To investigate the in vivo MMAE release, hQNM-PLGA NPs (7 mg MMAE/kg) were injected intratumorally to 4T1 tumor-bearing mice when the tumor volume was ~200, 500 and 800 mm^3. After 4 h or 8 h post injection, the tumors were collected, washed with PBS, and homogenized with lysis buffer on ice. MMAE was extracted with a methanol/DCM mixture solution and subjected to HPLC analysis as described above.

Detection of Hypoxia in Tumors

To evaluate the hypoxic level of tumor, 4T1 tumor-bearing mice with various tumor volume were intraperitoneally treated with pimonidazole (60 mg/kg). After 1 h post injection, tumors were collected, frozen, sectioned, stained with an anti-pimonidazole antibody (1:200) before fluorescence microscope observation.

Effects of NM-PLGA NPs on CTC-Neutrophil Cluster Formation and CTC Transendothelial Migration

To evaluate the effect of NPs on the formation of CTC-neutrophil cluster, 4T1 cells (1×10^5/well) were stained with hoechst 33258 and DiD, and diluted with mouse peripheral blood to simulate the environment of peripheral blood. In order to simulate the process of CTC circulation in blood, cells were incubated with calcein-AM labeled neutrophils and NM-PLGA NPs (10 μg PLGA/mL) for 1 h in a cell constant temperature shaken incubator. Cells were collected by centrifugation (1000 rpm, 5 min), cultured on cell crawls in 24-well plates for 6 h before confocal laser scanning microscope (CLSM) observation. Meanwhile, the NPs-treated cells were washed with PBS, collected and analyzed by for flow cytometry.

In order to investigate the transendothelial migration of CTCs, human umbilical vein endothelial cells (HUVECs) were grown in the upper chamber for 30 h. 4T1 cells, NM-PLGA NPs (10 μg PLGA/mL) and neutrophils were seeded into the upper chamber and co-incubated for 12 h. The migrated 4T1 cells were fixed before fluorescence microscope observation.

Cellular Uptake

4T1 cells were seeded at 5×10^4 cells/well into 12-well plates and cultured overnight. CNM-PLGA NPs and C-PLGA NPs (10 μg Cou6/mL) were added. After incubation for 4 h, the cells were washed with PBS, and stained with DAPI before CLSM observation. Besides, after treatment with different NPs for 8 h, the 4T1 cells were washed with PBS, collected and analyzed by flow cytometry. Alternatively, after treatment with C-PLGA NPs or CNM-PLGA NPs for different time, 4T1 cells were lysed for 20 min at RT. The content of Cou6 and protein in the mixture was measured by spectrophotometry (λ_{ex} = 466 nm, λ_{em} = 504 nm) and BCA kit, respectively.

In vitro Antitumor Efficacy

To evaluate the biosafety of NPs, 4T1 cells were seeded on 96-well plates at 8000 cells/well and cultured for 24 h. PLGA NPs, NM-PLGA NPs were added at various NP concentrations, and the cells were incubated for 96 h to assess cell viability by MTT assay.

To investigate the in vitro antitumor efficacy of NPs, 4T1 cells were seeded in 96-well plates at 8000 cells/well and incubated for 24 h. Free MMAE, hQ-PLGA NPs and hQNM-PLGA NPs were added at various MMAE concentrations. Cells were incubated for 96 h under normoxic or hypoxic (5% O_2) condition before viability assessment by MTT assay.

To observe dead/live cells, 4T1 cells were plated in 12-well plates at 3×10^4 cells/well and cultured overnight. hQ-PLGA NPs and hQNM-PLGA NPs (100 nM MMAE) were added and subjected to incubation with cells under normoxic or hypoxic (5% O_2) condition. After incubation for 96 h, cells were stained with calcein-AM (10 μM) and propidium iodide (5 μM) before fluorescence microscope observation.

Tumor Accumulation

Free DiR, D-PLGA NPs and DNM-PLGA NPs (1 mg DiR/kg) were i.v. injected to 4T1 tumor-bearing mice (~100 mm^3), respectively. The in vivo imaging system was used to obtain fluorescence imaging at different time points post-injection.

Moreover, the major tissues and tumors were collected at 8 h post injection, and further observed via in vivo imaging system (λ_{ex} = 748 nm, λ_{em} = 780 nm).

In vivo Antitumor and Anti-Metastasis Efficacy

The 4×10^6 4T1 cells were transplanted on the mammary fat pad of mice. The 4T1 tumor-bearing mice (~100 mm^3) were treated with PBS, free MMAE (2 mg MMAE/kg), hQ-PLGA NPs, hQNM-PLGA NPs (7 mg hQ-$MMAE_2$/kg) on days 1, 5 and 9 (n = 8). The tumor volume, body weight and survival rate of the mice were measured and recorded every 2 days. The major organs and tumors were collected on day 18, and subjected to H&E and TUNEL staining as previous report.[53]

The 4×10^6 Luc/GFP-4T1 cells were transplanted on the mammary fat pad of mice. The Luc/GFP-4T1 tumor-bearing mice (~100 mm^3) were treated with PBS, free MMAE (2 mg MMAE/kg), hQ-PLGA NPs, hQNM-PLGA NPs (7 mg hQ-$MMAE_2$/kg) on days 1, 5 and 9 (n = 8). Tumor metastases were monitored via the bioluminescence imaging mode of in vivo imaging system on days 0, 11, 22. D-fluorescein potassium salt (150 mg/kg) was injected intraperitoneally prior to each imaging. On day 22, the lungs were collected and subjected to H&E staining. Besides, blood was collected from mice on day 22, and the CTCs were isolated from blood using Histopaque-1077.[54] The collected CTCs incubated on coverslips for 6 h before fluorescence microscope observation.

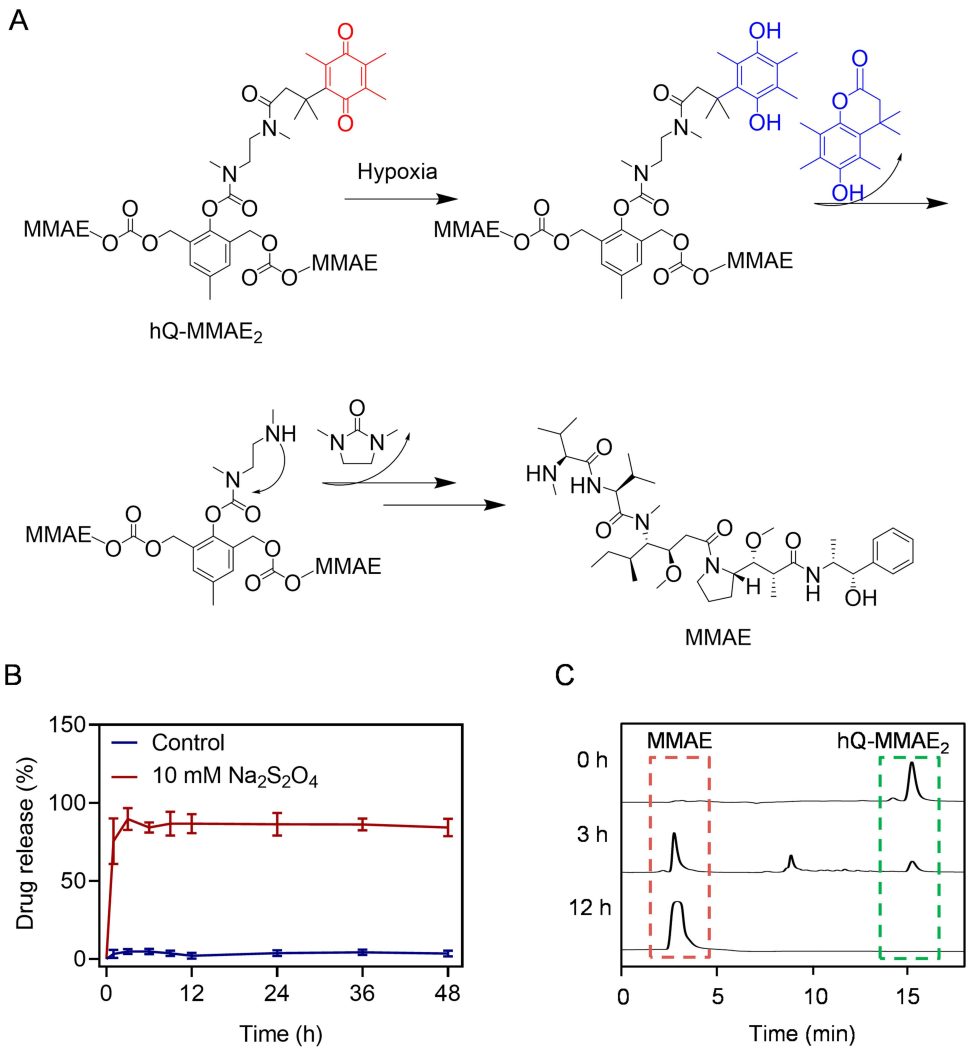

Figure 1 hQ-$MMAE_2$ degradation (**A**) The mechanism of hQ-$MMAE_2$ degradation. (**B**) MMAE release from hQ-$MMAE_2$ in the presence of 10 mM $Na_2S_2O_4$ (n = 3). (**C**) HPLC analysis of hQ-$MMAE_2$ degradation in the presence of 10 mM $Na_2S_2O_4$.

Statistical Analysis

Data could be expressed as mean ± standard deviation. The Student's *t*-test was used for statistical comparisons. The differences were set to be significant at *p < 0.05 and very significant at **p < 0.01 and ***p < 0.001.

Results and Discussion

Characterization and Degradation of hQ-MMAE$_2$

The synthesis and characterization of compound 2–10 and hQ-MMAE$_2$ were shown in Supporting Information (Scheme S1, Figures S3–S7). To limit fast MMAE aggregation during the formulation, the hypoxia-responsive dimeric prodrug, hQ-MMAE$_2$ was synthesized, wherein a flexible N, N'-dimethylethylene-diamine linker was incorporated between MMAE and hypoxia-responsive quinone to disrupt the MMAE–MMAE interaction and control MMAE release, thereby achieving high drug loading. On the other hand, the hQ-MMAE$_2$ degradation was analyzed by HPLC. When the $Na_2S_2O_4$ (a reducing agent) concentration was 10 mM, hQ-MMAE$_2$ degraded quickly, resulting in cumulative release reached 89% within 3 h (Figure 1A and B). The similar results were further evidenced by HPLC analysis (Figure 1C).

Preparation and Characterization of NPs

To prepare the neutrophil membrane (NM) coated NPs, the NM was isolated from neutrophils, and further coated on the surface of the hQ-PLGA NPs to obtain hQNM-PLGA NPs. The DLC and DLE of hQ-MMAE$_2$ in hQ-PLGA NPs were 29.4% and 93.7%, respectively, indicating that hQ-PLGA NPs have a high drug loading capacity. Besides, the particle size and zeta potential of hQ-PLGA NPs were 140 nm and −11 mV, respectively (Figure 2A). When the NM was coated

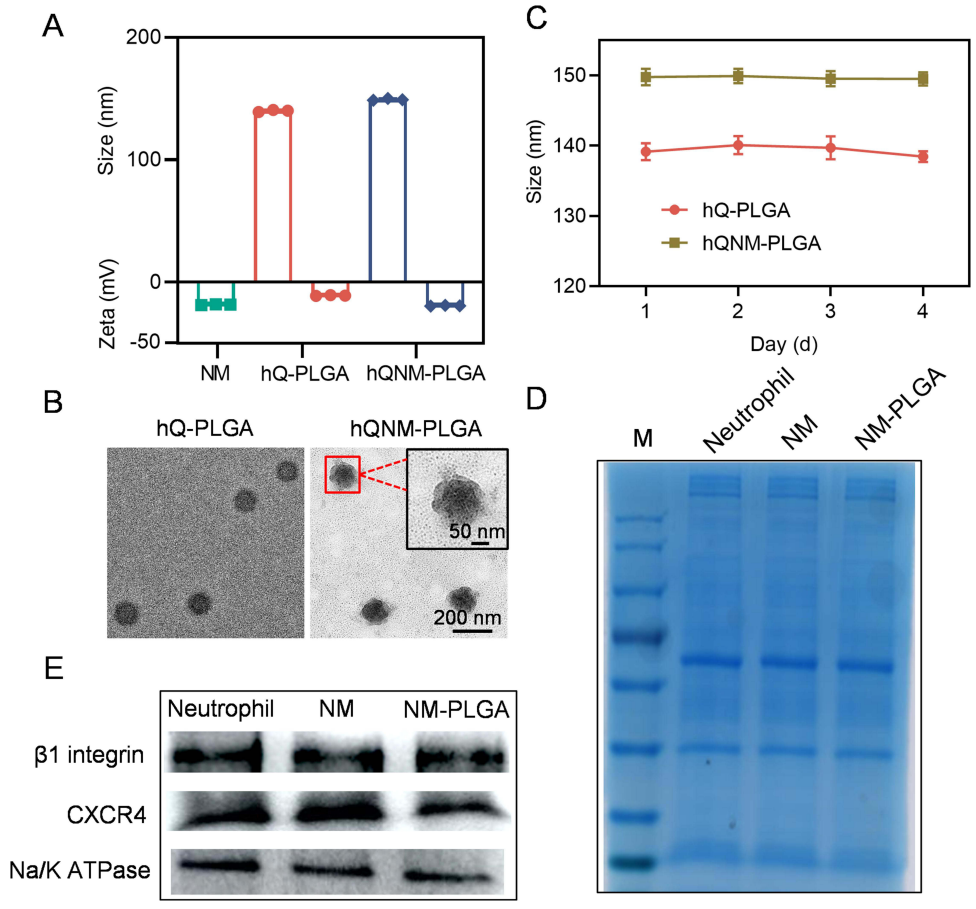

Figure 2 NPs characterization. (**A**) Size and zeta potential of NM, hQ-PLGA NPs and hQNM-PLGA NPs (n = 3). (**B**) TEM images of hQ-PLGA NPs and hQNM-PLGA NPs. (**C**) Stability of hQ-PLGA NPs and hQNM-PLGA NPs in PBS. (**D**) SDS-PAGE pattern of proteins from neutrophil, neutrophil membrane and NM-PLGA NPs. (**E**) Characteristic protein expression in neutrophil, neutrophil membrane and NM-PLGA NPs.

on the surface of hQ-PLGA NPs, the particle size of hQNM-PLGA NPs was slightly elevated to 149 nm, and the zeta potential was reduced to −19.2 mV, which was similar to the NM (−18.7 mV). Similar with DLS measurement, the TEM images also showed that hQNM-PLGA NPs possessed a spherical core-shell morphology and the particle size was 142 nm (Figure 2B). In addition, the NM coating improved the NP stability and inhibited the NP aggregation in PBS during the 4 days, as evidenced by minimal change in particle size (Figure 2C).

Alternatively, SDS-PAGE and Western blotting were performed to investigate whether NM coated on the surface of PLGA NPs. As shown in Figure 2D, the protein track of NM-PLGA NPs was consistent with that of the neutrophil and NM, suggesting that NM has successfully coated onto NPs. Moreover, Western blotting further confirmed that NM-PLGA NPs had the similar adhesion molecules protein (β1 integrin, CXCR4) expression as neutrophil and NM (Figure 2E). These results all indicated that the biomimetic NM surface was formulated.

Hypoxia-Induced MMAE Release in vitro and in vivo

To evaluate the MMAE release under various hypoxic condition (10% O_2, 5% O_2), 4T1 cells were incubated with hQ-PLGA NPs in hypoxic incubator for different time. As shown in Figure 3A, more MMAE released from hQ-PLGA NPs treated cells under hypoxic condition, where the MMAE level under hypoxic condition (5% O_2) was 4.6-fold higher than that under normoxic condition (20% O_2) after treatment for 12 h, indicating that the intracellular hypoxic condition could elicit MMAE release from hQ-PLGA NPs.

The hypoxic level of tumor with various tumor volume was measured by immunofluorescence staining. Compared to tumor with the volume of ~200 mm^3, the green fluorescence of hypoxyprobe was remarkably increased when the tumor volume increased to ~800 mm^3, which suggested that the advanced 4T1 tumors with larger tumor volume possessed serious hypoxic condition (Figure 3B). Furthermore, the quantitative HPLC analysis was subjected to monitor MMAE release in tumors with

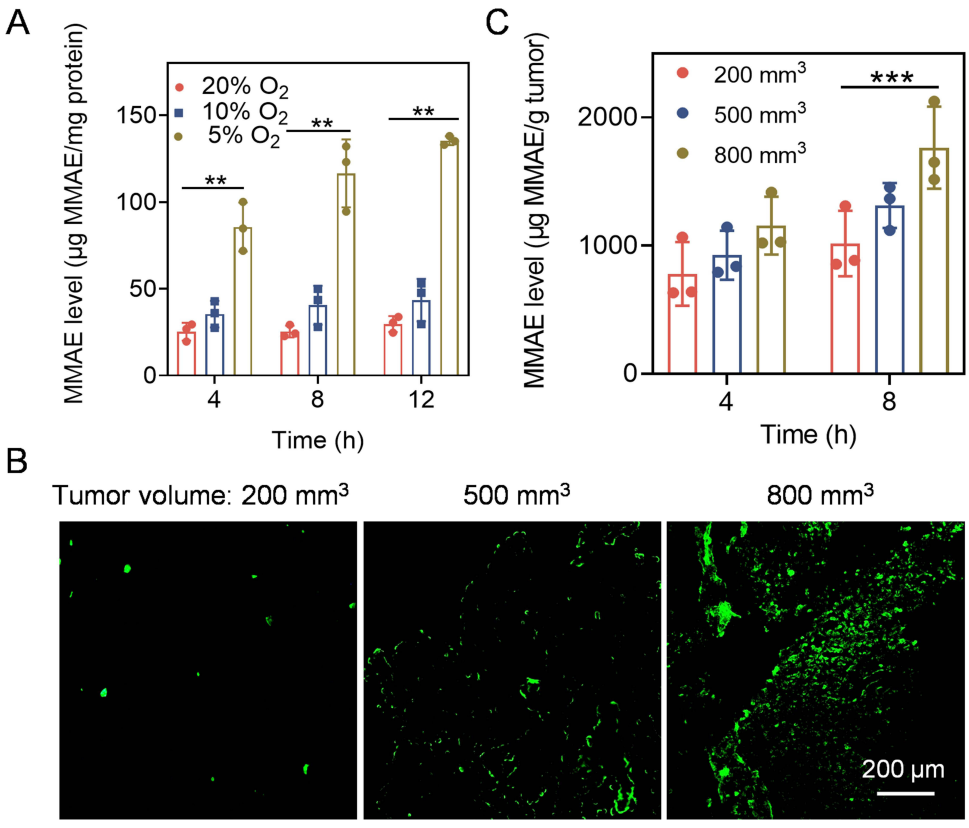

Figure 3 Hypoxia-induced MMAE release in vitro and in vivo. (**A**) The MMAE level in 4T1 cells incubated with hQNM-PLGA NPs under different oxygen levels (n = 3). (**B**) Immunofluorescence imaging of tumor sections stained with HypoxyprobeTM RedAPC Kit (hypoxia probe). (**C**) The MMAE level in hQNM-PLGA NPs treated 4T1 tumors with various tumor volume (n = 3). Data expressed as means ± SD. **p < 0.01; ***p < 0.001.

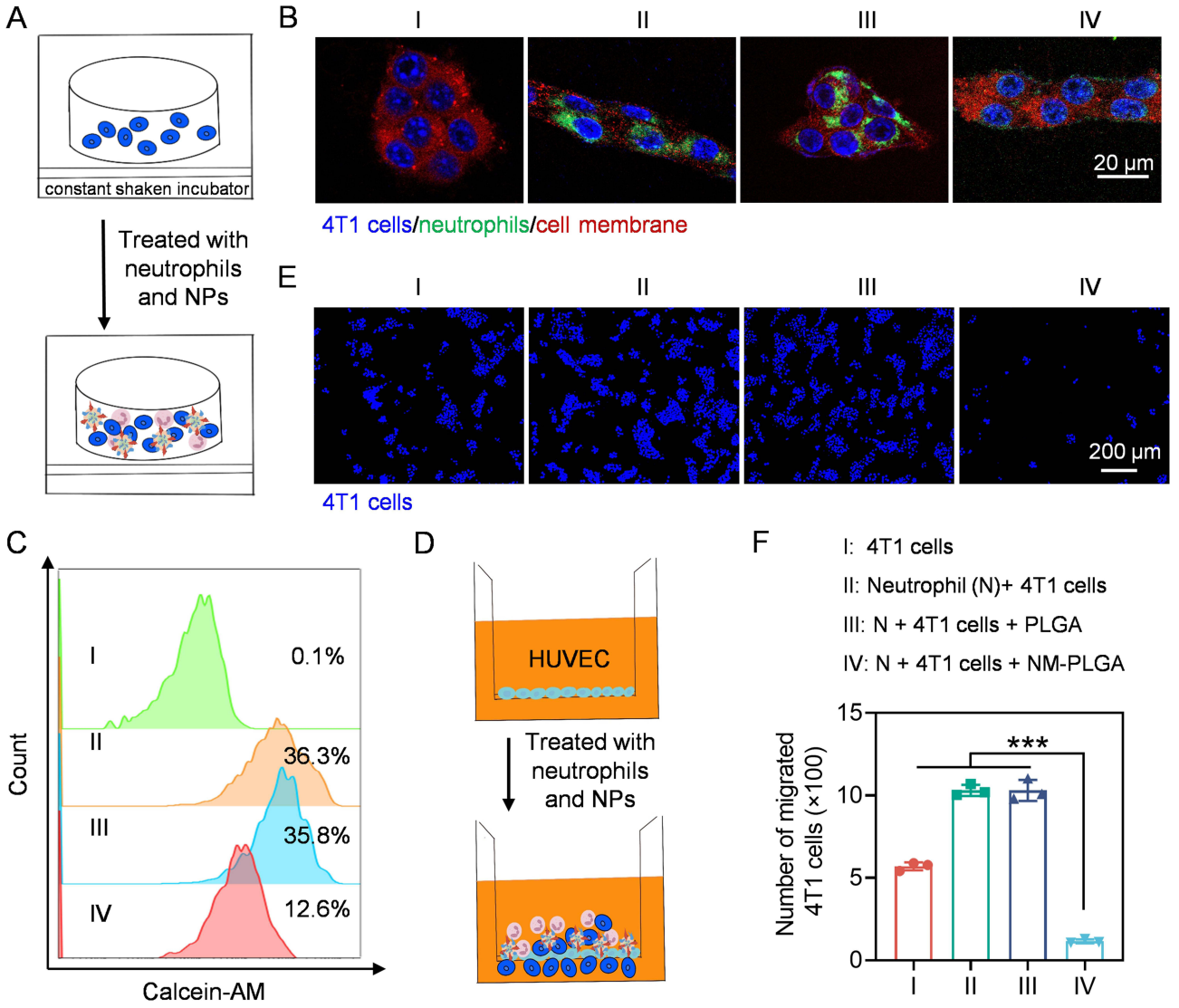

Figure 4 Inhibition of CTC-neutrophil cluster formation and CTCs transendothelial migration. (**A**) Schematic illustration of adhesion assay. (**B**) Fluorescence images of 4T1 cells incubated with neutrophils under different groups treatment. (**C**) Flow cytometric analysis of neutrophils-adhered 4T1 cells treated as described in (**B**). (**D**) Schematic illustration of migration assay. Fluorescence images (**E**) and number (**F**) of migrated 4T1 cells upon different groups treatment (n = 3). (I: 4T1 cells; II: Neutrophil (N)+ 4T1 cells; III: N + 4T1 cells + PLGA; IV: N + 4T1 cells + NM-PLGA) Data expressed as means ± SD. ***p < 0.001.

several tumor volume. After 8 h post-injection, the MMAE content in tumor (~800 mm^3) was higher than that with the volume of ~200 mm^3, indicating that advanced 4T1 tumors with larger tumor volume could facilitate MMAE release (Figure 3C). These results consistently demonstrated that the advanced 4T1 tumors possessed acute hypoxic environment and could notably trigger MMAE release.

Inhibition of CTC-Neutrophil Cluster Formation and CTCs Transendothelial Migration

The formation of CTC-neutrophil cluster upon NM-PLGA NPs treatment was assessed via CLSM observation. As shown in Figure 4A and B, a large overlap of green fluorescence (calcein-AM stained neutrophil) and red fluorescence (DiD-stained cell membrane) was demonstrated when 4T1 cells incubated with neutrophils in a cell shaken incubator, indicating that neutrophils could adhere to CTCs to form CTC-neutrophil cluster. However, minimal neutrophils could adhere to 4T1 cells with NM-PLGA NP treatment, as evidenced by low distribution of green fluorescence, suggesting that NM-PLGA NPs could serve as a competitor for neutrophils to disrupt the formation of neutrophils-CTC cluster. The similar conclusion could also be obtained by flow cytometry analysis (Figure 4C).

We further evaluated the effect of NM-PLGA NPs on tumor cell migration via in vitro migration assays. After incubation with neutrophils under NM-PLGA NP treatment, fewer 4T1 cells migrated compared to other groups (Figure 4D–F), suggesting that NM-PLGA NPs could effectively attenuate the migration ability of 4T1 cells. These results collectively verified that NM-PLGA NPs could effectively interrupt the formation of neutrophils-CTC cluster, thus attenuating the transendothelial migration ability of 4T1 cells to inhibit tumor metastasis.

Cellular Uptake

We further evaluated the targeted drug delivery of NM-PLGA NPs via CLSM observation. Compared to C-PLGA NPs-treated cells, large green fluorescence was distributed in cells treated with CNM-PLGA NPs (Figure 5A), suggesting that CNM-PLGA NPs had remarkable targeting ability to tumor cells. Besides, the cellular uptake level was further measured via spectrofluorimetry and flow cytometry. Excitingly, CNM-PLGA NPs consistently demonstrated higher uptake level

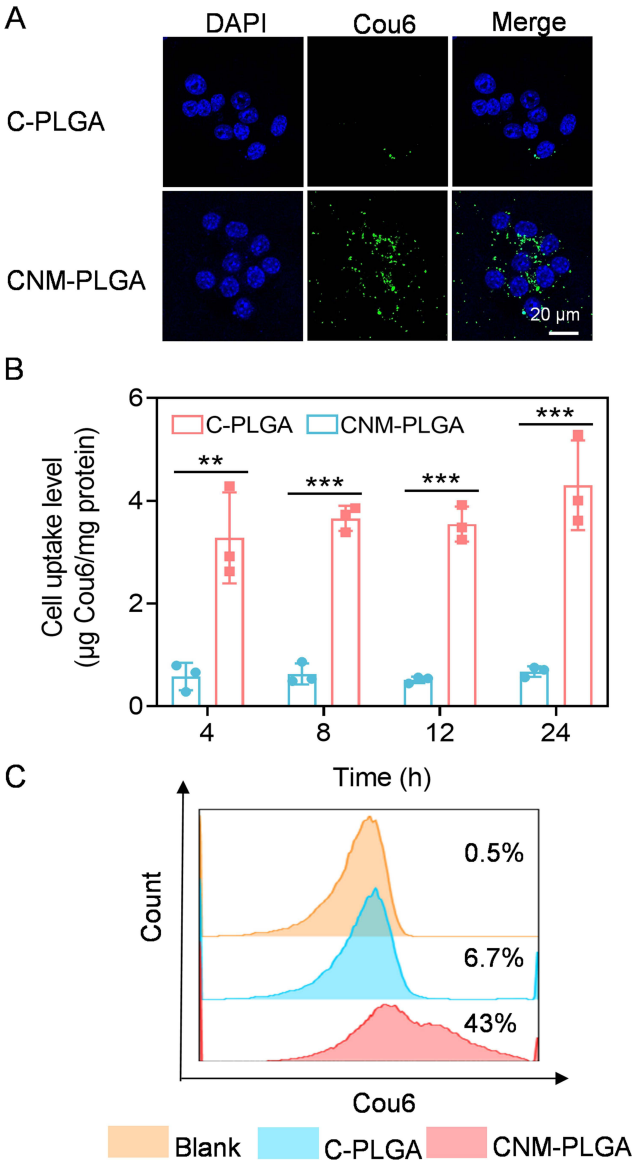

Figure 5 Cellular uptake. (**A**) CLSM images of 4T1 cells incubated with C-PLGA NPs, CNM-PLGA NPs for 4 h. (**B**) The cellular uptake level of Cou6 in 4T1 cells after incubation with CNM-PLGA NPs for 4 h, 8 h, 12 h and 24 h (n = 3). (**C**) Uptake level of Cou6 analysed by flow cytometry. The 4T1 cells were treated with various NPs for 8 h. Data expressed as means ± SD. **p < 0.01; ***p < 0.001.

compared to C-PLGA NPs (Figure 5B and C). These results consistently suggested that NM-PLGA NPs afforded notable in vitro targeting ability to 4T1 cells.

In vitro Antitumor Efficacy

To investigate the biosafety of NPs, cells were incubated with PLGA NPs or NM-PLGA NPs for 96 h. As shown in Figure 6A, over 90% cell viability was observed, indicating a good biosafety of NM-PLGA NPs. When 4T1 cells were co-incubated with various groups for 96 h under normoxic or hypoxic environment, the anti-tumor effect of hQNM-PLGA NPs was stronger than that of hQ-PLGA NPs, where the IC_{50} of MMAE in hQNM-PLGA NPs was >4.3-fold lower than in hQ-PLGA NPs (Figure 6B and C, Table S1). At the same time, the IC_{50} of MMAE in hQNM-PLGA NPs was significantly decreased under hypoxic condition compared to normoxic environment (Table S1). Alternatively, the calcein-AM/PI staining demonstrated that hQNM-PLGA NPs were able to cause more cell death (70.8%) under hypoxic environment compared to hQ-PLGA NPs (27.6%) (Figure 6D). These results indicating that hypoxia could promote hQ-$MMAE_2$ degradation to release MMAE, thus leading an outstanding anti-tumor effect.

Tumor Accumulation

The tumor accumulation of NM-PLGA NPs was then monitored by the in vivo imaging system (IVIS). Compared to free DiR and D-PLGA NPs, DNM-PLGA NPs demonstrated prominent tumor accumulation ability, as evidenced by the stronger fluorescence intensity of DiR in DNM-PLGA NPs-treated tumors (Figures 7A and S8). Surprisingly, the fluorescence intensity of DiR reached the maximum value at 8 h post-injection. The similar results were also obtained in ex vivo imaging of tissues (Figure 7B and C). Collectively, these results suggested that neutrophil membrane coating could endow NPs with the property of tendency to inflammatory tumor, thus contributing to tumor accumulation of NM-PLGA NPs.

In vivo Antitumor and Anti-Metastasis Efficacy

The antitumor efficacy of NPs was evaluated using orthotopic 4T1 tumor bearing mice (Figure 8A). During 18 d treatment, hQ-PLGA NPs partially inhibited tumor growth, while hQNM-PLGA NPs had a significant inhibition effect

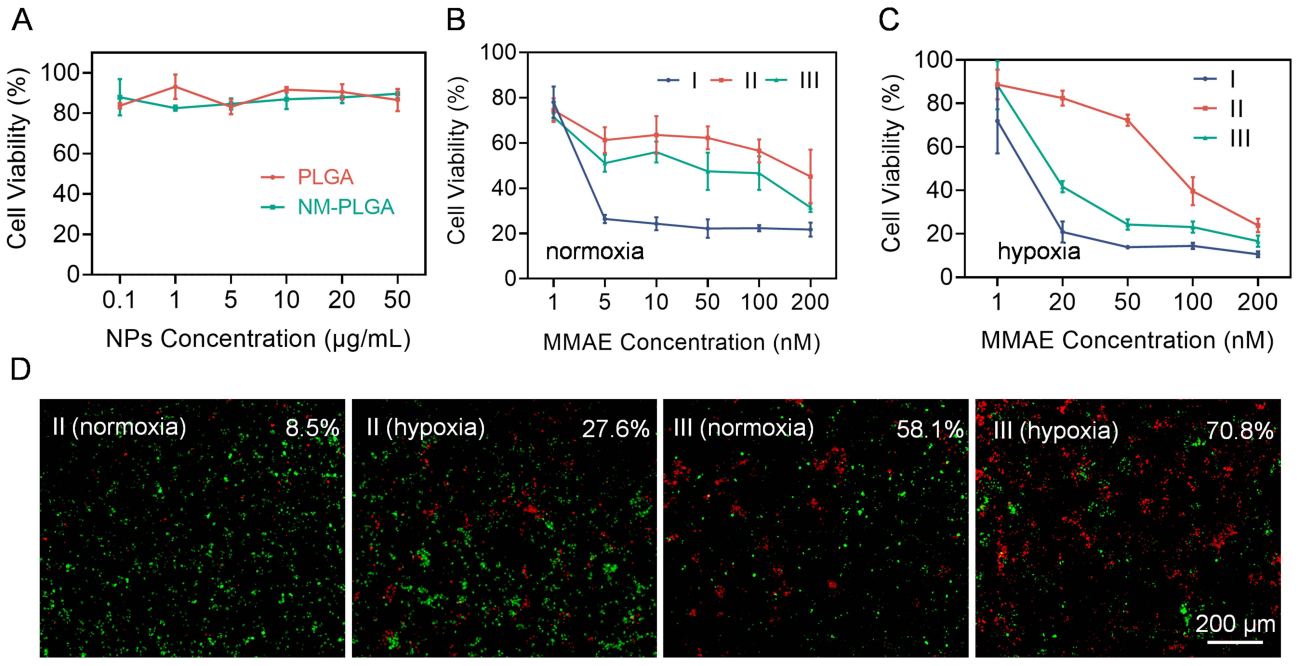

Figure 6 In vitro anticancer efficacy. (**A**) Biosafety of PLGA NPs and NM-PLGA NPs to 4T1 cells (n = 3). Viability of 4T1 cells incubated with various groups for 96 h under normoxic (**B**) or hypoxic (**C**) environment (n = 3). (**D**) Fluorescence images of 4T1 cells treated with hQ-PLGA and hQNM-PLGA NPs for 96 h under normoxic or hypoxic condition. (I: free MMAE; II: hQ-PLGA; III: hQNM-PLGA.).

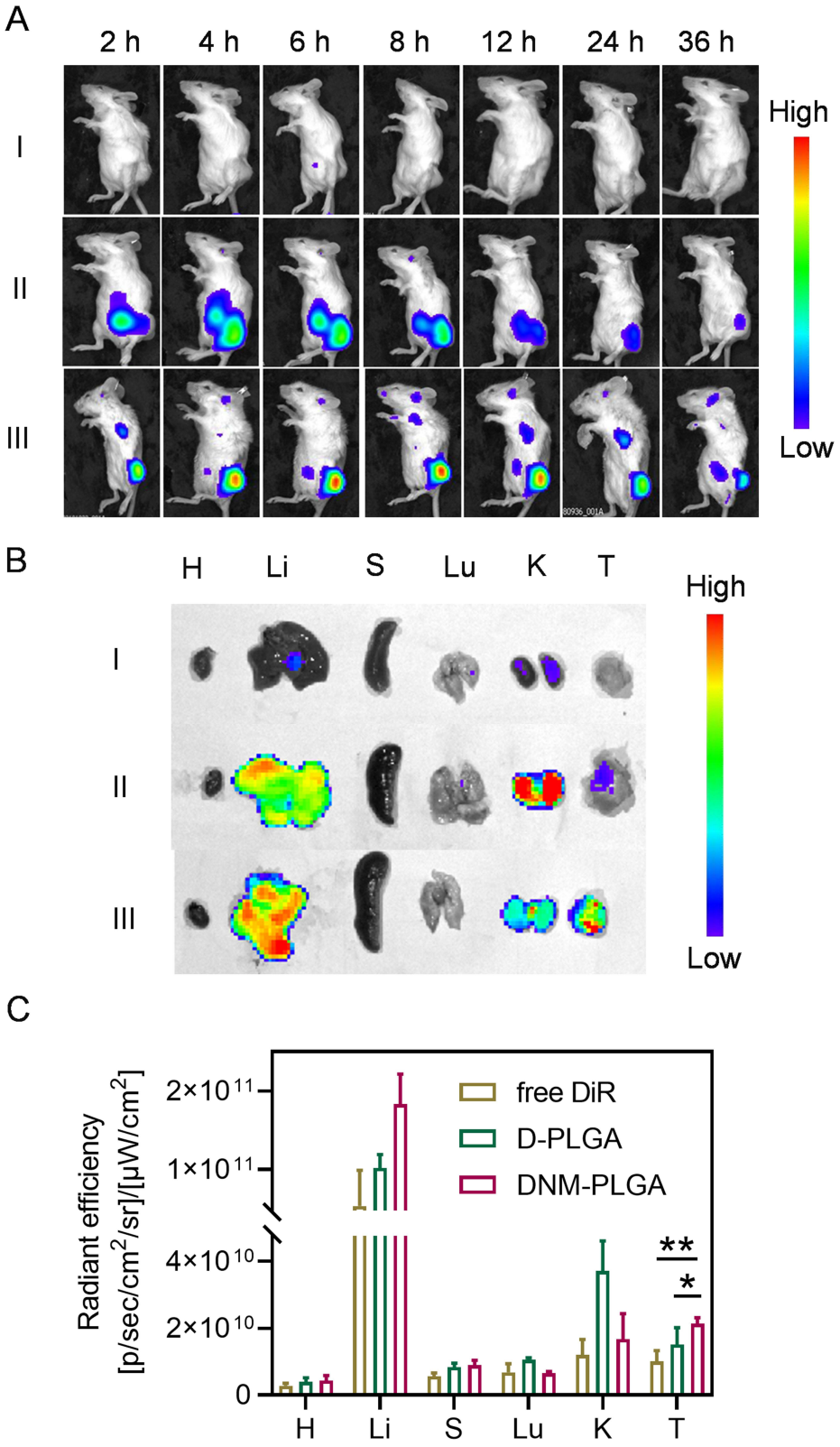

Figure 7 In vivo biodistribution. (**A**) Fluorescence imaging of mice after intravenous injection of different groups (I, free DiR; II, D-PLGA; III, DNM-PLGA). Fluorescence imaging (**B**) and intensity (**C**) of tumors and major organs at 8 h post injection (n = 3). Data expressed as means ± SD. *p < 0.05; **p < 0.01.
Abbreviations: H, heart; Li, liver; S, spleen; Lu, lung; K, kidney; T, tumor.

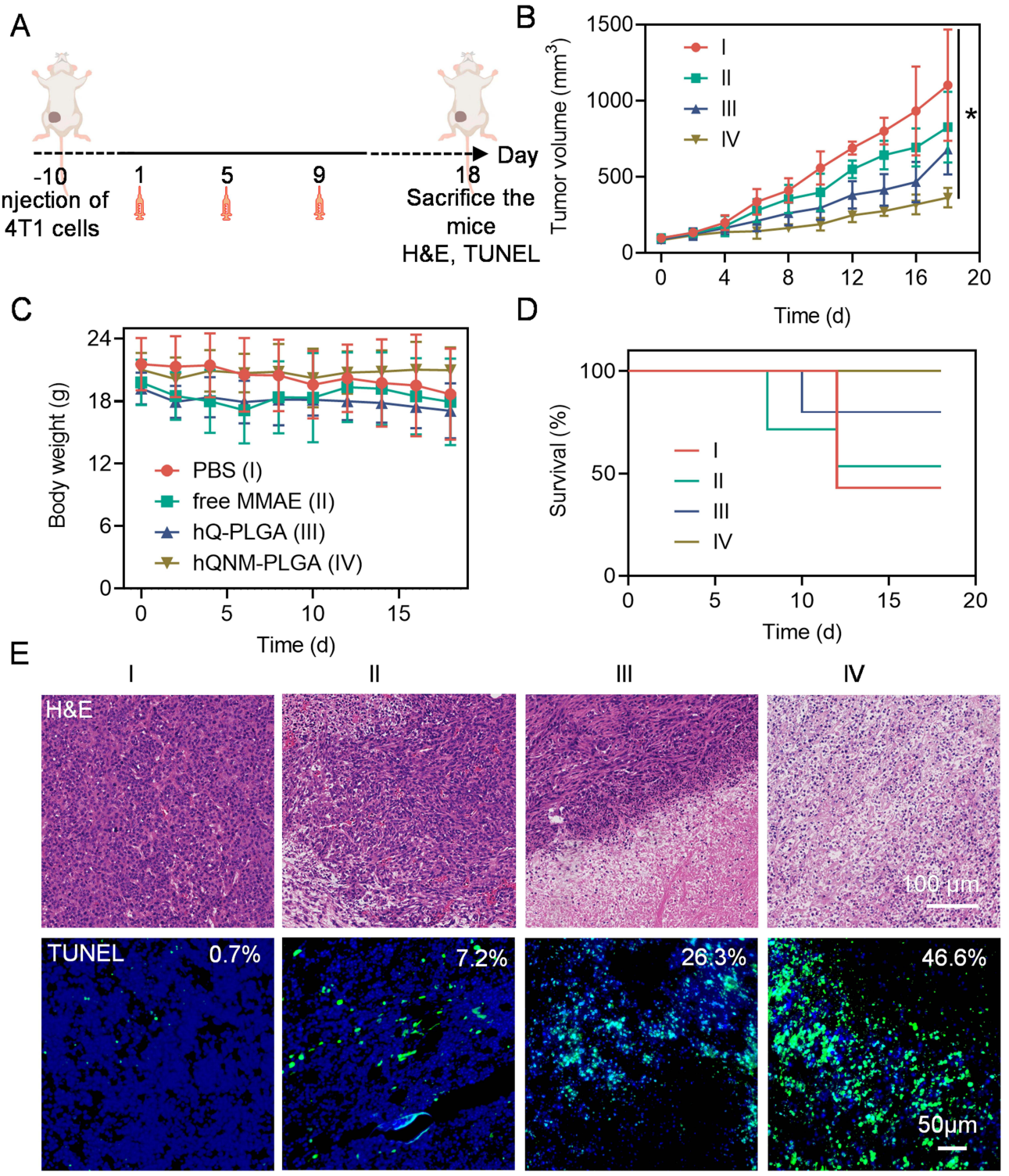

Figure 8 In vivo anticancer efficacy. (**A**) Schematic illustration demonstrating the treatment protocol. (**B**) Tumor growth curves. Body weight changes of mice (**C**) and survival rates (**D**) of mice injected with different groups (7 mg hQ-MMAE$_2$/kg, n = 8). (**E**) H&E and TUNEL staining of tumor harvested from mice on day 18. (I: PBS; II: free MMAE; III: hQ-PLGA; IV: hQNM-PLGA) Data expressed as means ± SD. *p < 0.05.

on tumor progression (Figures 8B and S9). Meanwhile, the H&E and TUNEL staining revealed that hQNM-PLGA NPs treated mice had the highest cell remission and apoptotic rate, thus resulting in highest survival rate (Figure 8D and E). On the other hand, there were negligible body weight and pathological changes in hQNM-PLGA NPs treated mice

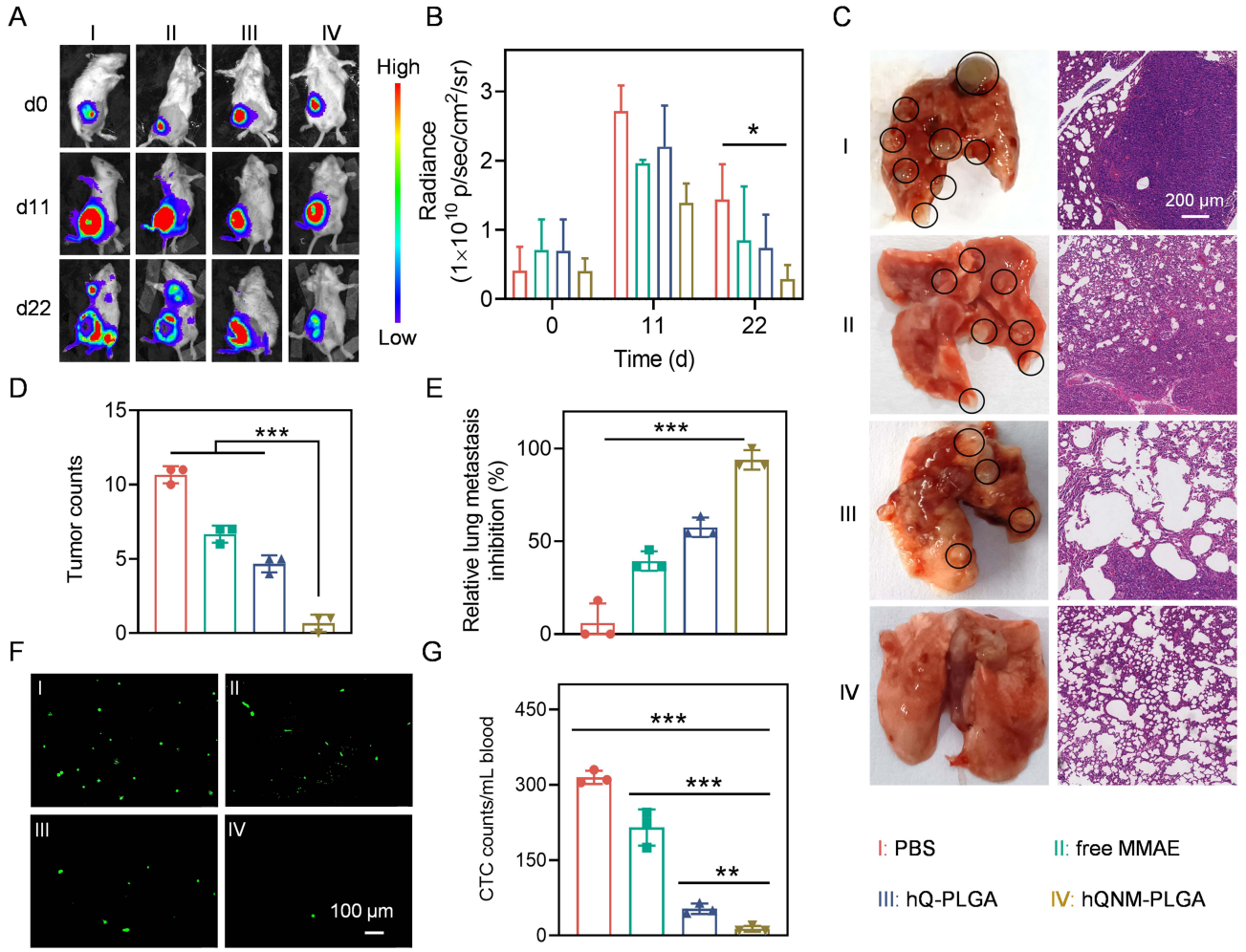

Figure 9 In vivo anti-metastasis efficacy. Representative bioluminescence images (**A**) and integrated bioluminescence intensity (**B**) of Luc/GFP-4T1 orthotopic mammary tumor-bearing mice on day 0, 11, 22 (7 mg hQ-MMAE$_2$/kg, n = 8). (**C**) H&E staining of lung collected from mice on day 22. The black circles refer to tumors. (**D**) Metastatic nodule counts on the lung tissues from different groups (n = 3). (**E**) The inhibition rate of different groups on lung metastasis (n = 3). Representative fluorescent images (**F**) and counts (**G**) of GFP$^+$ 4T1 cells isolated from mice on day 22 (n = 3). (I: PBS; II: free MMAE; III: hQ-PLGA; IV: hQNM-PLGA) Data expressed as means ± SD. *p < 0.05; **p < 0.01; ***p < 0.001.

(Figures 8C and S10), indicating good biocompatibility of NPs. Collectively, these results showed that hQNM-PLGA NPs could afford notable in vivo antitumor efficacy and safety.

The anti-metastasis efficacy of NPs was evaluated using orthotopic Luc/GFP-4T1 tumor bearing mice that could spontaneously metastasize to distant organs. To verify the anti-metastasis effect of hQNM-PLGA NPs, 4T1 metastases were monitored by in vivo IVIS imaging system during the treatment period. Compared with the PBS group, the bioluminescence signals in the whole body were significantly reduced in the hQNM-PLGA NP treatment group (Figure 9A and B), suggesting perfect anti-metastasis efficacy of hQNM-PLGA NPs. Alternatively, CTCs and lung were isolated from each group of mice on day 22. In consistence with above results, the hQNM-PLGA NPs treated mice had the minimal tumor nodules and metastatic lesions in lung, and few number of CTCs in whole blood (Figure 9C–G). Collectively, these results indicated that hQNM-PLGA NPs could effectively inhibit tumor growth and metastasis.

Conclusion

In summary, we designed a neutrophil membrane-camouflaged, hypoxia-responsive nanomedicine (hQNM-PLGA NPs) with high drug loading for multi-site cancer and anti-metastasis therapy. First, we successfully synthesized the hypoxia-sensitive hQ-MMAE$_2$, which can successfully degrade and release free MMAE in hypoxic environment in vitro and in vivo. Western blot assay demonstrated that hQNM-PLGA NPs have intact adhesion proteins on their surface and

possess neutrophil properties, thus hQNM-PLGA NPs can successfully target drug delivery to tumor sites for the elimination of primary tumor. Alternatively, hQNM-PLGA NPs could serve as the competitor for neutrophils to disrupt the formation of CTC-neutrophil cluster, leading to a reduction in the transendothelial migration ability of CTCs to prevent tumor metastasis. At the end of the treatment of in situ tumors in mice, the hQNM-PLGA NP treatment group possessed the highest survival rate, the highest metastasis inhibition rate and the fewest metastatic nodules in the lungs, as well as the lowest levels of CTCs in the blood of mice, achieving good anti-tumor therapeutic effects and inhibition of lung metastasis. Thus, this multi-site attack, biomimetic nano-platform offers a new possibility for anti-cancer treatment and metastasis inhibition.

Acknowledgments

This work was supported by the Young TopNotch Talents Foundation of Henan Agricultural University (30500737), the National Natural Science Foundation of China (51903074), the Key Technologies R&D Program of Henan Province (212102310252).

Disclosure

The authors report no conflicts of interest in this work.

References

1. Mohme M, Riethdorf S, Pantel K. Circulating and disseminated tumour cells — mechanisms of immune surveillance and escape. *Nat Rev Clin Oncol*. 2017;14(3):155–167. doi:10.1038/nrclinonc.2016.144
2. Miller KD, Nogueira L, Mariotto AB, et al. Cancer treatment and survivorship statistics, 2019. *CA Cancer J Clin*. 2019;69(5):363–385. doi:10.3322/caac.21565
3. Shen S, Xu X, Lin S, et al. A nanotherapeutic strategy to overcome chemotherapeutic resistance of cancer stem-like cells. *Nat Nanotechnol*. 2021;16(1):104–113. doi:10.1038/s41565-020-00793-0
4. Sun T, Zhang YS, Pang B, Hyun DC, Yang M, Xia Y. Engineered nanoparticles for drug delivery in cancer therapy. *Angew Chem Int Ed Engl*. 2014;53(46):12320–12364. doi:10.1002/anie.201403036
5. Kopeček J, Yang J. Polymer nanomedicines. *Adv Drug Deliv Rev*. 2020;156:40–64. doi:10.1016/j.addr.2020.07.020
6. Zhou Q, Dong C, Fan W, et al. Tumor extravasation and infiltration as barriers of nanomedicine for high efficacy: the current status and transcytosis strategy. *Biomaterials*. 2020;240:119902. doi:10.1016/j.biomaterials.2020.119902
7. Ni Q, Zhang F, Liu Y, et al. A bi-adjuvant nanovaccine that potentiates immunogenicity of neoantigen for combination immunotherapy of colorectal cancer. *Sci Adv*. 2020;6(12):eaaw6071. doi:10.1126/sciadv.aaw6071
8. Wang YF, Kohane DS. External triggering and triggered targeting strategies for drug delivery. *Nat Rev Mater*. 2017;2(6):17020. doi:10.1038/natrevmats.2017.20
9. Tang L, Wang Z, Mu Q, et al. Targeting neutrophils for enhanced cancer theranostics. *Adv Mater*. 2020;32(33):2002739. doi:10.1002/adma.202002739
10. Shang B, Cui H, Xie R, et al. Neutrophil extracellular traps primed intercellular communication in cancer progression as a promising therapeutic target. *Biomark Res*. 2023;11(1):24. doi:10.1186/s40364-023-00463-y
11. Szczerba BM, Castro-Giner F, Vetter M, et al. Neutrophils escort circulating tumour cells to enable cell cycle progression. *Nature*. 2019;566(7745):553–557. doi:10.1038/s41586-019-0915-y
12. Saini M, Szczerba BM, Aceto N. Circulating tumor cell-neutrophil tango along the metastatic process. *Cancer Res*. 2019;79(24):6067–6073. doi:10.1158/0008-5472.Can-19-1972
13. Iriondo O, Yu M. Unexpected friendship: neutrophils help tumor cells en route to metastasis. *Dev Cell*. 2019;49(3):308–310. doi:10.1016/j.devcel.2019.04.021
14. Zhu K, Li P, Mo Y, et al. Neutrophils: accomplices in metastasis. *Cancer Lett*. 2020;492:11–20. doi:10.1016/j.canlet.2020.07.028
15. Kang T, Zhu Q, Wei D, et al. Nanoparticles coated with neutrophil membranes can effectively treat cancer metastasis. *ACS Nano*. 2017;11(2):1397–1411. doi:10.1021/acsnano.6b06477
16. Zhen X, Cheng P, Pu K. Recent advances in cell membrane-camouflaged nanoparticles for cancer phototherapy. *Small*. 2019;15(1):1804105. doi:10.1002/smll.201804105
17. Oroojalian F, Beygi M, Baradaran B, Mokhtarzadeh A, Shahbazi MA. Immune cell membrane-coated biomimetic nanoparticles for targeted cancer therapy. *Small*. 2021;17(12):e2006484. doi:10.1002/smll.202006484
18. Park JH, Mohapatra A, Zhou J, et al. Virus-mimicking cell membrane-coated nanoparticles for cytosolic delivery of mRNA. *Angew Chem Int Ed Engl*. 2022;61(2):e202113671. doi:10.1002/anie.202113671
19. Nguyen PHD, Jayasinghe MK, Le AH, Peng B, Le MT. Advances in drug delivery systems based on red blood cells and their membrane-derived nanoparticles. *ACS Nano*. 2023;17(6):5187–5210. doi:10.1021/acsnano.2c11965
20. Hao H, Chen Y, Wu M. Biomimetic nanomedicine toward personalized disease theranostics. *Nano Res*. 2021;14(8):2491–2511. doi:10.1007/s12274-020-3265-z
21. Zhang Y, Cai K, Li C, et al. Macrophage-membrane-coated nanoparticles for tumor-targeted chemotherapy. *Nano Lett*. 2018;18(3):1908–1915. doi:10.1021/acs.nanolett.7b05263

22. Jiang Q, Wang K, Zhang X, et al. Platelet membrane-camouflaged magnetic nanoparticles for ferroptosis-enhanced cancer immunotherapy. *Small*. 2020;16(22):e2001704. doi:10.1002/smll.202001704
23. Liu W, Ruan M, Wang Y, et al. Light-triggered biomimetic nanoerythrocyte for tumor-targeted lung metastatic combination therapy of malignant melanoma. *Small*. 2018;14(38):e1801754. doi:10.1002/smll.201801754
24. Bahmani B, Gong H, Luk BT, et al. Intratumoral immunotherapy using platelet-cloaked nanoparticles enhances antitumor immunity in solid tumors. *Nat Commun*. 2021;12(1):1999. doi:10.1038/s41467-021-22311-z
25. Kang H, Rho S, Stiles WR, et al. Size-dependent EPR effect of polymeric nanoparticles on tumor targeting. *Adv Healthc Mater*. 2020;9(1):e1901223. doi:10.1002/adhm.201901223
26. He J, Li C, Ding L, et al. Tumor targeting strategies of smart fluorescent nanoparticles and their applications in cancer diagnosis and treatment. *Adv Mater*. 2019;31(40):1902409. doi:10.1002/adma.201902409
27. Bonferoni MC, Rassu G, Gavini E, et al. Electrochemotherapy of deep-seated tumors: state of art and perspectives as possible "EPR effect enhancer" to improve cancer nanomedicine efficacy. *Cancers*. 2021;13(17):4437. doi:10.3390/cancers13174437
28. Wang YB, Wang Z, Xu CN, Tian HY, Chen XS. A disassembling strategy overcomes the EPR effect and renal clearance dilemma of the multifunctional theranostic nanoparticles for cancer therapy. *Biomaterials*. 2019;197:284–293. doi:10.1016/j.biomaterials.2019.01.025
29. Knoche SM, Larson AC, Sliker BH, Poelaert BJ, Solheim JC. The role of tumor heterogeneity in immune-tumor interactions. *Cancer Metastasis Rev*. 2021;40(2):377–389. doi:10.1007/s10555-021-09957-3
30. Zhuang WR, Wang Y, Cui PF, et al. Applications of π-π stacking interactions in the design of drug-delivery systems. *J Control Release*. 2019;294:311–326. doi:10.1016/j.jconrel.2018.12.014
31. Tang XH, Du XM, Yu YT, et al. Deep-penetrating triple-responsive prodrug nanosensitizer actuates efficient chemoradiotherapy in pancreatic ductal adenocarcinoma models. *Small*. 2022;18(31):2202834. doi:10.1002/smll.202202834
32. Zhu J, Guo T, Wang Z, Zhao Y. Triggered azobenzene-based prodrugs and drug delivery systems. *J Control Release*. 2022;345:475–493. doi:10.1016/j.jconrel.2022.03.041
33. Li X, Li W, Li K, et al. Albumin-coated pH-responsive dimeric prodrug-based nano-assemblies with high biofilm eradication capacity. *Biomater Sci*. 2023;11(3):1031–1041. doi:10.1039/d2bm01520j
34. Wang C, Wang Q, Wang H, et al. Hydroxyethyl starch-folic acid conjugates stabilized theranostic nanoparticles for cancer therapy. *J Control Release*. 2023;353:391–410. doi:10.1016/j.jconrel.2022.11.059
35. Wang H, Lu Q, Miao Y, et al. Boosting SN38-based oral chemotherapy to combine reduction-bioactivated structured lipid-mimetic prodrug with ascorbic acid. *Nano Res*. 2022;15(10):9092–9104. doi:10.1007/s12274-022-4544-7
36. Ju Y, Wang Z, Ali Z, et al. A pH-responsive biomimetic drug delivery nanosystem for targeted chemo-photothermal therapy of tumors. *Nano Res*. 2022;15(5):4274–4284. doi:10.1007/s12274-022-4077-0
37. Wang L, Dai C, Fang Y, You X, Wu J. A drug/carrier dual redox-responsive system based on 6-mercaptopurine dimer-loaded cysteine polymer nanoparticles for enhanced lymphoma therapy. *Nano Res*. 2022;15(5):4544–4551. doi:10.1007/s12274-021-4037-0
38. Song J, Cheng M, Xie Y, Li K, Zang X. Efficient tumor synergistic chemoimmunotherapy by self-augmented ROS-responsive immunomodulatory polymeric nanodrug. *J Nanobiotechnology*. 2023;21(1):93. doi:10.1186/s12951-023-01842-1
39. Lu M, Huang X, Cai XH, et al. Hypoxia-responsive stereocomplex polymeric micelles with improved drug loading inhibit breast cancer metastasis in an orthotopic murine model. *ACS Appl Mater Interfaces*. 2022;14(18):20551–20565. doi:10.1021/acsami.1c23737
40. He H, Chen Y, Li Y, et al. Effective and selective anti-cancer protein delivery via all-functions-in-one nanocarriers coupled with visible light-responsive, reversible protein engineering. *Adv Funct Mater*. 2018;28(14):1706710. doi:10.1002/adfm.201706710
41. Dutta D, Zhou Q, Mukerabigwi JF, Lu N, Ge Z. Hypoxia-responsive polyprodrug nanocarriers for near-infrared light-boosted photodynamic chemotherapy. *Biomacromolecules*. 2021;22(11):4857–4870. doi:10.1021/acs.biomac.1c01152
42. Zhou Q, Mohammed F, Wang Y, et al. Hypoxia-responsive block copolymer polyprodrugs for complementary photodynamic-chemotherapy. *J Control Release*. 2021;339:130–142. doi:10.1016/j.jconrel.2021.09.023
43. Choi J-S, Seo K, Yoo J-W. Recent advances in PLGA particulate systems for drug delivery. *J Pharm Investig*. 2012;42(3):155. doi:10.1007/s40005-012-0024-5
44. Pan L, Zhao W, Lai J, et al. Sortase a-generated highly potent anti-CD20-MMAE conjugates for efficient elimination of b-lineage lymphomas. *Small*. 2017;13(6):1602267. doi:10.1002/smll.201602267
45. Miller MA, Mikula H, Luthria G, et al. Modular nanoparticulate prodrug design enables efficient treatment of solid tumors using bioorthogonal activation. *ACS Nano*. 2018;12(12):12814–12826. doi:10.1021/acsnano.8b07954
46. Marcher A, Nijenhuis MAD, Gothelf KV. A wireframe DNA cube: antibody conjugate for targeted delivery of multiple copies of monomethyl auristatin e. *Angew Chem Int Ed Engl*. 2021;60(40):21691–21696. doi:10.1002/anie.202107221
47. Suski JM, Lebiedzinska M, Wojtala A, et al. Isolation of plasma membrane-associated membranes from rat liver. *Nat Protoc*. 2014;9(2):312–322. doi:10.1038/nprot.2014.016
48. Boxio R, Bossenmeyer-Pourie C, Steinckwich N, Dournon C, Nusse O. Mouse bone marrow contains large numbers of functionally competent neutrophils. *J Leukoc Biol*. 2004;75(4):604–611. doi:10.1189/jlb.0703340
49. He H, Chen S, Zhou J, et al. Cyclodextrin-derived pH-responsive nanoparticles for delivery of paclitaxel. *Biomaterials*. 2013;34(21):5344–5358. doi:10.1016/j.biomaterials.2013.03.068
50. Yang Y, Ding Y, Fan B, et al. Inflammation-targeting polymeric nanoparticles deliver sparfloxacin and tacrolimus for combating acute lung sepsis. *J Control Release*. 2020;321:463–474. doi:10.1016/j.jconrel.2020.02.030
51. Zhang Q, Dehaini D, Zhang Y, et al. Neutrophil membrane-coated nanoparticles inhibit synovial inflammation and alleviate joint damage in inflammatory arthritis. *Nat Nanotechnol*. 2018;13(12):1182–1190. doi:10.1038/s41565-018-0254-4
52. Su Y, Wang T, Su Y, et al. A neutrophil membrane-functionalized black phosphorus riding inflammatory signal for positive feedback and multimode cancer therapy. *Mater Horiz*. 2020;7(2):574–585. doi:10.1039/c9mh01068h
53. Wang Y, Huo J, Li S, et al. Self-rectifiable and hypoxia-assisted chemo-photodynamic nanoinhibitor for synergistic cancer therapy. *ACS Appl Mater Interfaces*. 2022;14(8):10092–10101. doi:10.1021/acsami.1c23121
54. Ding P, Wang Z, Wu Z, et al. Tannic acid (TA)-functionalized magnetic nanoparticles for EpCAM-independent circulating tumor cell (CTC) isolation from patients with different cancers. *ACS Appl Mater Interfaces*. 2021;13(3):3694–3700. doi:10.1021/acsami.0c20916